AIAA JOURNAL
Vol. 44, No. 12, December 2006

Propagation Speed, Internal Energy, and Direct Aeroacoustics Simulation Using Lattice Boltzmann Method

X. M. Li,* R. M. C. So,† and R. C. K. Leung‡
Hong Kong Polytechnic University, Hung Hom, Kowloon, Hong Kong, People's Republic of China

DOI: 10.2514/1.18933

The validity of the lattice Boltzmann method for direct aeroacoustics simulations depends on its ability to correctly recover the equation of state of the gas and its dynamic viscosity. This paper presents a lattice Boltzmann method with two relaxation times to carry out the direct aeroacoustics simulations of a two-dimensional Gaussian sound pulse in a uniform flow over a range of Mach numbers (M) varying from 0.01 to 0.9. It is assumed that there is no shock present in the range of Mach numbers tested. A sixth-order finite-difference scheme is used to evaluate the convective term in the modeled Boltzmann equation, and a second-order Runge–Kutta scheme is used to forward march in time. Thus solved, the calculations show that the wave propagation speed (c) over the range $0.01 \leq M \leq 0.9$, determined from the deduced equation of state and from the propagation of the pulse, are in good agreement with theoretical analysis and direct numerical simulation results obtained by solving the unsteady compressible Navier–Stokes equations using a low-dispersive and low-dissipative finite-difference scheme. The specific heat ratio (γ) for a diatomic gas is recovered correctly and so is the dependence of the internal energy on γ. Thus, the proposed lattice Boltzmann method is valid for direct aeroacoustics simulations at very low to near transonic M.

I. Introduction

THE development of computational aeroacoustics essentially centers around two approaches [1]. One is based on the application of the acoustic analogy or hybrid approach to the time-dependent computational fluid dynamics data. Another, known as direct noise computation or direct aeroacoustics simulation (DAS), is based on the simultaneous calculation of the aerodynamic and acoustic fields obtained by solving the unsteady compressible Navier–Stokes equations plus the perfect gas equation of state. The solutions of these two approaches are different. The first approach yields the noise radiation in the far field, but the second approach could, in addition, provide a better understanding of the noise source mechanisms. Furthermore, the DAS would also provide the link between turbulence dynamics and the acoustic waves. However, this understanding is obtained at the expense of serious numerical issues that may be difficult to overcome [1,2].

In the first approach, the aerodynamic field is solved using one of three different methods: direct numerical simulation (DNS), large eddy simulation (LES), and Reynolds averaged Navier–Stokes (RANS) modeling of the turbulence field. These methods solved the governing flow equations including the equation of state of the fluid with no attempt made to resolve the acoustics scales, which are, in general, 2 orders of magnitude smaller than the aerodynamic scales. The unsteady compressible Navier–Stokes equations are solved for a wide range of flow scales with no assumptions made on the turbulence field in the DNS approach. In the case of LES, the Navier–Stokes equations explicitly filtered in space are solved with a subgrid-scale turbulence model for the near-wall region. On the other hand, the RANS solution is based on a suitable turbulence model for the whole flowfield. Once the time-dependent solution of the aerodynamic field is available, velocity fluctuations can be introduced directly into the integral appearing in the inhomogeneous wave equation of Lighthill [3] to estimate the radiated acoustic field. Alternatively, velocity fluctuations can be input to the linearized Euler equations [4,5] to obtain an estimate of the noise source and the radiated acoustic field. In the acoustic analogy or hybrid approach, the wave equation in one form or another is solved. This means that the propagation speed of sound is specified and is not calculated as part of the solution.

In the DAS approach, the unsteady compressible Navier–Stokes equations and the gas equation of state are solved simultaneously using DNS, thus allowing the acoustic field and the aerodynamic field to be determined without modeling the source terms in the wave equation. This is accomplished through the use of a mesh that includes the acoustic field. Because aerodynamic noise is represented by very small amplitude fluctuations compared with flow fluctuations, typically $u'_{\text{acous}}/u'_{\text{aero}}$ is of order 10^{-3} to 10^{-4} and $p'_{\text{acous}}/p'_{\text{aero}}$ is of order 10^{-2} for a jet at a Mach number $M = 0.9$, the length scale separation between these two fields is large, of the order of 10^2. Here, u' is the fluctuating velocity and p' is the fluctuating pressure; the subscripts "acous" and "aero" denote acoustic and aerodynamic field, respectively. Therefore, a low-dispersive and a low-dissipative numerical scheme is required if the acoustic waves propagating in the computational domain are to be preserved correctly [1,2,6,7]. Besides, there are other complicating issues involved in the inflow and outflow boundary conditions. At these boundaries, the assumed computational boundaries should allow the aerodynamic field to pass freely with minimal reflection while at the same time they should be nonreflecting for the incident acoustic waves. Otherwise, the spurious erroneous waves reflecting from the boundaries would contaminate the numerical simulations, decrease the computational accuracy, and might even drive the solutions towards a wrong time-stationary state. Practical approaches to deal with these issues have been discussed and proposals made to remedy the difficulties. Among the more promising proposals [8] are the Navier–Stokes characteristics-based boundary conditions (NSCBC) [9], the absorbing boundary condition (ABC) [10], and the method of perfectly matched layer [11]. These proposals have been applied to numerous problems, including jet flow and duct flow with geometric discontinuities [12–15]. Therefore, DAS is a viable approach to estimate far field noise and its source mechanisms in the study of aeroacoustic problems.

Recently, the lattice Boltzmann method (LBM), which is derived from the lattice gas automata, has been proposed as an alternative to

Received 19 July 2005; revision received 6 September 2006; accepted for publication 13 September 2006.

*Ph.D. Student, Department of Mechanical Engineering.
†Emeritus Professor, Department of Mechanical Engineering, and the Industrial Center. Fellow AIAA.
‡Assistant Professor, Department of Mechanical Engineering. Senior Member AIAA.

conventional computational fluid dynamics techniques [16,17]. Since then, LBM has been used to tackle a variety of fluid dynamics problems ranging from single-component hydrodynamics to multiphase flows to flow through porous media to flows with reaction and diffusion, etc. However, development of LBM for single-phase compressible flow, such as air, has received particular attention because all LBM proposed can recover the macroscopic unsteady compressible Navier–Stokes equations [18,19]. Some recent proposals were even made to simulate compressible flows and wave propagation [20–24], thus allowing DAS to be carried out. Other proposals based on the lattice kinetic equation [25] and the direct simulation Monte Carlo [26] have also been put forward. All these proposals are not very satisfactory for DAS because they have drawbacks of one type or another. First, it is not clear whether the wave propagation speed c could be estimated correctly as the Mach number $M \to 0$, even though the LBM with an assumed collision model is shown to be correct in the incompressible limit [27] and has been applied to simulate incompressible turbulent jets [28]. Second, some proposals [20] yield a dynamic viscosity coefficient μ that varies linearly with temperature whereas others [22,23] assume monoatomic gas particles with a constant specific heat ratio of $\gamma = 1.67$. Third, the gas equation of state is recovered but not always correctly [29,30]. Consequently, the validity of these proposals for a true DAS is questionable. Other methods have also been put forward for compressible flow with sound waves propagation [29] and wave propagation with shock [30] buildup. These proposals give rise to a speed of sound given by $c^2 = p/\rho$, where p is the thermodynamic pressure and ρ is the gas density, thus implying that $\gamma = 1$ for a perfect diatomic gas. As yet, there is no single proposal that could recover the gas equation of state's μ, γ, and c correctly for a wide range of M. If the LBM were to be a true alternative to the DNS as a viable DAS technique, its ability to recover the gas equation of state's μ, γ, and c correctly is most desirable.

Therefore, it is necessary to develop a LBM, the performance of which is comparable to the DNS in a direct simulation of aeroacoustic problems. If this objective were to be achieved, it is essential that the gas equation of state's μ, γ, and c be recovered correctly for a perfect gas, such as air, for a range of M varying from the incompressible limit to finite M. Such a proposal [31] has been put forth recently. The proposal demonstrates that the gas equation of state's μ and γ could be calculated accurately for a diatomic gas at finite M. However, it is not clear whether μ, γ, and the internal energy e could be recovered correctly in the limit of $M \to 0$. The present objective is to show that c and the theoretical relation between c and e can also be recovered exactly over a range of M ranging from the incompressible limit to transonic flow. A Gaussian sound pulse in a uniform flow is used as the vehicle to demonstrate the validity and extent of the proposed LBM, and the results are calibrated against theoretical analysis and DNS calculations of the same problem.

In the next section, the DNS solution of the governing unsteady compressible Navier–Stokes equations and the perfect gas equation of state is briefly described. Details of the low-dispersive and low-dissipative numerical method used have been fully discussed [7] and were also described elsewhere [31,32]. This is followed by a discussion of the proposed LBM, the time scales, and the lattice used. Numerical solution of the LBM governing equations is obtained by using the same low-dispersive and low-dissipative scheme. The results of the numerical simulations of a Gaussian sound pulse in a uniform flow are presented over a range of M varying from 0.01 to 0.9 in Sec. IV. Finally, the conclusions drawn are summarized in Sec. V.

II. Direct Numerical Simulation Solution

The unsteady compressible Navier–Stokes equations in strong conversation form and the equation of state $p = \rho RT$ for a perfect gas (in this case air) in two dimensions are made dimensionless using $U_\infty, L_\infty, \rho_\infty, \mu_\infty$, and T_∞ as reference quantities for velocity, length, density, dynamic viscosity, and temperature, respectively, where R is the universal gas constant. The reference time is given by L_∞/U_∞, the reference pressure by $\rho_\infty U_\infty^2$, and the reference internal energy by U_∞^2. Thus normalized, the Reynolds number at an upstream inlet is $Re = \rho UL/\mu$. Here, the dimensionless pressure, density, velocity, length, time, internal energy, and dynamic viscosity are denoted by p, ρ, u, l, t, e, and μ, respectively. In the following discussion all quantities are expressed in dimensionless form unless otherwise specified. The nondimensional governing equations are solved by a five-point sixth-order compact finite-difference scheme suggested by Lele [7] to obtain the spatial derivative and an explicit fourth-order Runge–Kutta scheme for time marching. High-order filtering of Visbal and Gaitonde [33] is applied in every final stage of the Runge–Kutta scheme to suppress numerical instabilities due to spatial differencing. Because the present calculations are carried out over open space with no solid boundaries, NSCBC is applied to close the governing equations at all boundaries. Together, this constitutes the low-dispersive finite-difference scheme used to obtain solutions over the range $0.01 \le M \le 0.9$.

Central finite-difference schemes are generally dispersive and dissipative. Their resolutions of high-frequency fluctuations are poor. The low-dispersive and low-dissipative nature of the present scheme is verified by analyzing the spatial Fourier transform of the waveform of the Gaussian sound pulse. According to Hu et al. [34], the maximum resolvable dimensionless effective wave-number $k_c^* \Delta x$ for the present scheme is 1.36 and the maximum stable effective wave number is $k_{\max}^* \Delta x = 2.0$, where Δx is the dimensionless spacing of a uniform mesh. This is determined using a criterion $|k^* \Delta x - k\Delta x| < 0.005$, where $k\Delta x$ is the true wave number. In other words, the scheme can resolve only long waves with a low cutoff wavelength around $0.217/\Delta x$. For shorter wavelengths, the numerical dispersion due to finite differencing will be significant. Altogether, nine cases with M varying from 0.01 to 0.9 (see Table 1) are calculated. The Reynolds number at the inlet is taken to be 1.0×10^3 for all cases studied. The flow can still be assumed to be laminar with this choice of Reynolds number; therefore, there is no need to complicate the computations with the assumption of turbulence modeling. An effective way to ascertain whether the propagation of the Gaussian pulse is properly resolved and free from numerical dispersion is to trace the variation of its Fourier components in wave-number space during calculation. It was observed that all the Fourier components in each calculation do not show observable change during propagation, and their distributions in all nine cases are essentially identical. A sample distribution of Fourier components of pulse density fluctuation ρ_{k^*} versus the dimensionless effective wave-number $k^* \Delta x$ is shown in Fig. 1. The Δx chosen is independent of M and is taken to be 0.1. On the other hand, Δt varies from 2×10^{-7} to 1×10^{-4} for the range $0.01 \le M \le 0.9$. It is found that this choice of Δx and Δt gives very stable calculations over the range of M investigated. It can be seen that the power spectral density (PSD) is essentially zero beyond $k^* \Delta x = 1.36$. Therefore, it can be concluded that the low-dispersive and low-dissipative scheme of Lele [7] can be used to simulate a Gaussian sound pulse in a uniform flow. It will be shown later that the c and e thus recovered are in excellent agreement with theoretical results over the M range studied.

Table 1 Comparison of the numerically calculated c with its theoretical value

M	0.01	0.0125	0.02	0.05	0.1	0.3	0.5	0.7	0.9
Theoretical c	100	80	50	20	10	3.33	2	1.43	1.11
LBM/DNS calculated c	100	80	49.75	20.25	10.2	3.33	2	1.45	1.14
Error, %	0	0	0.5	1.25	2	0	0	1.39	2.7

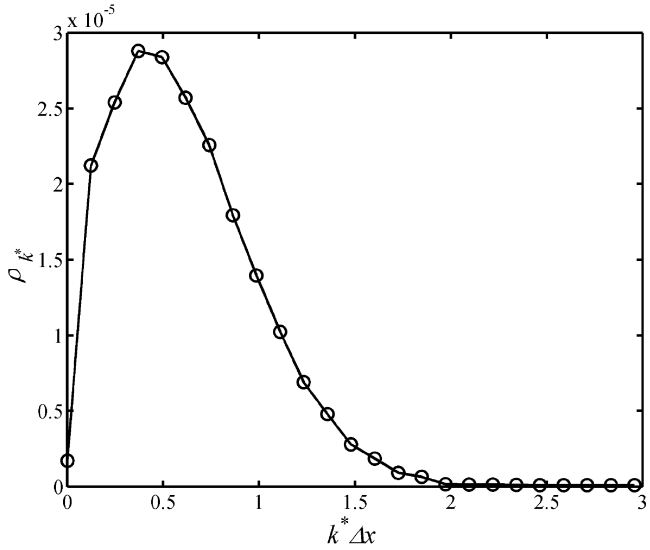

Fig. 1 PSD of the effective wave-number $k^*\Delta x$: LBM, circles; DNS, solid line.

III. Lattice Boltzmann Method Simulation

A. Conventional Lattice Boltzmann Method

The LBM adopted here is based on the conventional LBM in which the collision function is approximated by the commonly used Bhatnagar–Gross–Krook (BGK) model [35]. The derivation of this LBM/BGK has been described in detail elsewhere [19,22,36]; therefore, only the salient features are highlighted here. The LBM is based on the modeled solution of the continuous Boltzmann equation (BE) that describes the evolution of the distribution function f of a cloud of particles in a fluid. The BE can be written as

$$\frac{\partial f}{\partial t} + \boldsymbol{\xi} \cdot \nabla f + \boldsymbol{F}_{\text{ex}} \cdot \nabla_{\xi} f = Q(f, f) \tag{1}$$

where $f(x, \boldsymbol{\xi}, t)$ is the probability of finding a gas particle at location $\boldsymbol{x}$ moving with microscopic velocity $\boldsymbol{\xi}$ at time t, $\boldsymbol{F}_{\text{ex}}$ indicates external body force due to gravity or of electromagnetic origin, and the operator Q accounts for the binary particle collision occurring within a differential collision cross section. Equation (1) is difficult to solve because Q involves the integral of f over the velocity space as well as over the collision cross-sectional space. Consequently, Eq. (1) becomes a very complicated integral–differential equation whose solution up to now could be obtained only by appropriately modeling Q.

In the conventional approach, $\boldsymbol{F}_{\text{ex}} = 0$ and the popular BGK kinetic model with a single relaxation time is adopted for Q. Consequently, Q in Eq. (1) can be replaced by $-(f - f^{\text{eq}})/\tau\phi$, where τ is the relaxation time, ϕ is the relaxation time factor, f is the distribution function, and f^{eq} is its equilibrium value given by the Maxwell–Boltzmann distribution function

$$f^{\text{eq}} = \frac{\rho}{(2\pi RT)^{D/2}} \exp\left(-\frac{|\boldsymbol{\xi} - \boldsymbol{u}|^2}{2RT}\right) \tag{2}$$

Here, D is the dimension number, 2 for two-dimensional (2D) and 3 for three-dimensional (3D) flows. According to Ferziger and Kaper [37], from the kinetic theory point of view, single relaxation time is tantamount to the adoption of a rigid sphere collision model. The modeled Eq. (1) could then be discretized in the velocity space and a 9-bit square lattice model usually denoted as D2Q9 is used to simulate 2D flows. It is shown that the unsteady compressible Navier–Stokes equations are recovered correctly with the transport coefficients and pressure given by

$$\mu = \left(\phi - \frac{1}{2}\right)\frac{2}{D}\rho e\tau \tag{3}$$

$$\kappa = \frac{DR}{2}\kappa' = (\phi - 1)\frac{(D+2)R}{D}\rho e\tau \tag{4}$$

$$p = \frac{2}{D}\rho e \tag{5}$$

$$c = \sqrt{\frac{\gamma p}{\rho}} = \sqrt{\frac{2(D+2)}{D^2}e} \tag{6}$$

$$\gamma = \frac{D+2}{D} \tag{7}$$

where κ and κ' are the fluid thermal conductivity and diffusivity, respectively. It is obvious that the transport coefficients are related to D; therefore, the results yield a correct gas equation of state for 3D flows with $\gamma = 1.4$ but an incorrect state equation with $\gamma = 2$ for 2D flows. Furthermore, $\phi > 1/2$ has to be chosen if the condition of positivity of the transport coefficients has to be realized.

B. Modified Lattice Boltzmann Method

The conventional LBM/BGK has drawbacks, and the sound speed thus calculated will be in error for 2D flows. To remedy these drawbacks, the conventional BGK model has to be revisited. One possible alternative is to consider relaxing the rigid sphere collision model. In general, a polyatomic gas can undergo translational, rotational, and vibrational motions. If a proper macroscopic internal energy were to be defined, both translational and rotational motions have to be taken into account. Using D_T to denote the degree of freedom of translational motion and D_R to signify the degree of freedom of rotational motion, the total number of degrees of freedom for a diatomic gas like air is given by $D_T + D_R = 5$. Some measurable macroscopic averages of the flow, such as ρ, $\rho\boldsymbol{u}$, e, and p, can be defined from the velocity moments of the distribution function, where bold letters are used to denote velocity vectors and the parameters are all normalized by the reference scales defined above. These expressions can be written as

$$\rho = \int f \, \mathrm{d}\boldsymbol{\xi} \tag{8}$$

$$\rho\boldsymbol{u} = \int \boldsymbol{\xi} f \, \mathrm{d}\boldsymbol{\xi} \tag{9}$$

$$\rho e + \frac{1}{2}\rho|\boldsymbol{u}|^2 = \frac{D_T + D_R}{D_T}\int \frac{1}{2} f|\boldsymbol{\xi}|^2 \, \mathrm{d}\boldsymbol{\xi} \tag{10}$$

$$\left(\rho e + p + \frac{1}{2}\rho|\boldsymbol{u}|^2\right)\boldsymbol{u} = \frac{D_T + D_R}{D_T}\int \frac{1}{2} f|\boldsymbol{\xi}|^2\boldsymbol{\xi} \, \mathrm{d}\boldsymbol{\xi} \tag{11}$$

Integration of Eq. (10) suggests an explicit internal energy definition $e = (D_T + D_R)RT/2$ for diatomic gas, and Eq. (11) can then be used to determine p once e is known. Therefore, it can be seen that the total number of degrees of freedom of gas molecular motions plays an important role in the determination of p and e.

The added degrees of freedom could be incorporated into the derivation of the unsteady compressible Navier–Stokes equations in the following manner. If the conventional BGK model [35] with slight modification is assumed for Q and $\boldsymbol{F}_{\text{ex}}$ is again taken to be zero for the cases studied here, Eq. (1) can be rewritten as

$$\frac{\partial f}{\partial t} + \boldsymbol{\xi} \cdot \nabla_{\mathbf{x}} f = -\frac{1}{\tau_{\text{eff}}}(f - f^{\text{eq}}) \tag{12}$$

where τ_{eff} is an effective relaxation time and would reduce to τ in the case of the conventional BGK model. The relaxation time, irrespective of τ or τ_{eff}, is usually much smaller than the gas particle movement time. This disparity in time scales could be exploited in the derivation of the unsteady compressible Navier–Stokes equations and their transport coefficients from the Boltzmann Eq. (12) by means of the Chapman–Enskog expansion [38]. The expansion is about the Knudsen number ε, which is defined as the ratio of the mean free path between two successive particle collisions and the characteristic spatial scale of the fluid system. Typically, ε is a very small number and terms of order ε^2 can be neglected. Thus derived, the unsteady compressible Navier–Stokes equations can be recovered, and the transport coefficients of the fluid can be written as [31]

$$\mu = (\gamma - 1)\rho e \tau_{\text{eff}} \tag{13}$$

$$\lambda = -(\gamma - 1)^2 \rho e \tau_{\text{eff}} \tag{14}$$

$$\kappa' = \gamma(\gamma - 1)\rho e \tau_{\text{eff}} \tag{15}$$

where γ and the gas equation of state are given by

$$\gamma = \frac{D_T + D_R + 2}{D_T + D_R} \tag{16}$$

$$p = \frac{2\rho e}{D_T + D_R} = (\gamma - 1)\rho e = \rho RT \tag{17}$$

The relation between sound speed c and e then follows:

$$c^2 = \frac{\gamma p}{\rho} = \gamma(\gamma - 1)e \tag{18}$$

Because $D_T + D_R = 5$, $\gamma = 1.4$; therefore, γ and the relation between c and e are recovered. This formulation requires the transport coefficients to be a function of τ_{eff}. If $\tau_{\text{eff}} = \tau$ is assumed, it gives rise to $\mu \propto T^{1/2}$ even after the translational and rotational degrees of freedom are considered in the collision model [31]. The question then is how to formulate τ_{eff} so that at least μ could be rendered consistent with Sutherland's law.

The incorrect μ dependence on T could be remedied by considering the phenomenon of fluid viscosity, which could be interpreted as the result of momentum transfer between gas particles before and after collisions. The distributions of particle momenta depend on the individual particle momentum when they are far apart and on the intermolecular potentials when they are close to each other. The intermolecular potentials could be modeled by assuming the molecules as rigid spheres. However, this model alone would lead to the single relaxation time given in Eq. (12) and an incorrect estimate of μ. Sutherland (see Ferziger and Kaper [37]) suggested the inclusion of a weak but rapidly decaying repulsive potential in modeling particle interactions and obtained a more realistic representation of the dependence of μ on T. This weak interaction effect could be accounted for in the proposed LBM by postulating a relaxation time for the weak repulsive potential. The relaxation times for the intermolecular potential and for the weak repulsive potential are then used to determine τ_{eff} for Eq. (12). The correct form for τ_{eff} could be gleaned from the functional form of Sutherland's law. If this form were to be recovered correctly, $\tau_{\text{eff}} = \tau_1/(1 + \tau_1/\tau_2)$ has to be defined, where $\tau_1 = \tau$ is the relaxation time associated with the conventional BGK model and τ_2 is the relaxation time associated with the weak repulsive potential. Thus derived, μ can be shown to be given by

$$\mu = \rho RT \tau_{\text{eff}} = \frac{\rho RT}{(1/\tau_1 + 1/\tau_2)} \tag{19}$$

According to Ferziger and Kaper [37], τ_1 could be estimated from the rigid sphere model and the result gives $\tau_1 \propto T^{-1/2}$. The relaxation time τ_2 could be deduced by requiring the derived μ to have T dependence as that given by Sutherland's law. It can be shown that $\tau_1/\tau_2 = S_0/T$, where S_0 is the Sutherland constant. Because $\tau_1 \propto T^{-1/2}$, $\tau_2 \propto T^{1/2}$ follows immediately from $\tau_1/\tau_2 = S_0/T$, and both relaxation times are known. Therefore, the modified LBM solves Eq. (12) with two relaxation times rather than one and gives the correct gas equation of state's γ and μ.

C. Numerical Scheme

Only a brief description of the numerical method is given in the following discussion because the scheme has been described in other references [31,39]. The discretized form of Eq. (12) is solved. The equation is discretized in a velocity space using a finite set of velocity vectors $\{\boldsymbol{\xi}_i\}$ whereas the Maxwell–Boltzmann equilibrium function f^{eq} is expanded in a Taylor series of $\boldsymbol{\xi} \cdot \boldsymbol{u}$ such that

$$f^{\text{eq}} = \rho A_i \left\{ 1 + \frac{\boldsymbol{\xi} \cdot \boldsymbol{u}}{\theta} + \frac{(\boldsymbol{\xi} \cdot \boldsymbol{u})^2}{2\theta^2} - \frac{\boldsymbol{u}^2}{2\theta} - \frac{(\boldsymbol{\xi} \cdot \boldsymbol{u})\boldsymbol{u}^2}{2\theta^2} + \frac{(\boldsymbol{\xi} \cdot \boldsymbol{u})^3}{6\theta^3} + O\left(\frac{\boldsymbol{u}^4}{\theta^2}\right) \right\} \tag{20}$$

where $\boldsymbol{u} = (u, v)$, $\theta = RT$, and the weighting factors A_i are dependent on the assumed lattice model used to represent the discrete velocity space. The weighting factors are estimated from the constraints imposed on the evaluation of the local macroscopic flow variables. The term on the right-hand side of Eq. (12) is evaluated locally at every time step, whereas the second term on the left–hand side of Eq. (12) is estimated using a sixth-order finite-difference scheme similar to that proposed by Lele [7]. A second-order Runge–Kutta time marching scheme is used to calculate the time-dependent term in Eq. (12).

For the 2D diatomic gas problems studied here, two different velocity lattices have been tested, and these are the D2Q9 and the D2Q13 models. For the present calculation, δt for the lattice motion is chosen to be the same as Δt for time marching, and the grid size Δx is again taken to be the same as that used in the DNS scheme. It is also assumed the same for all M cases calculated. To obtain stable numerical solutions for all M considered, the lattice size δx has to be chosen so that $\delta x/\delta t \approx c$. This choice of c yields very stable numerical solutions for the whole range of M investigated. The validity was found to be true for both the D2Q9 and the D2Q13 models. Like the calculations reported previously [31,39], the D2Q13 model was found to give more accurate results, and it was used throughout this investigation.

Essentially, the numerical scheme adopted is similar to that used to carry out the DNS simulation. Furthermore, the same Δx and Δt are adopted. Therefore, it is also a low-dispersive and low-dissipative scheme. This fact can be gleaned from a comparison of the DNS and the LBM numerical simulation results of a Gaussian sound pulse in a uniform stream and the resultant PSD determined from the waveform. A typical plot of the PSD versus the dimensionless wave number is shown in Fig. 1. The DNS and LBM results are essentially identical, thus lending evidence to support the claim that the proposed LBM scheme is also suitable for DAS.

IV. Numerical Results and Discussion

Both DNS and LBM schemes are used to simulate the aerodynamic and acoustic fields created by a Gaussian sound pulse in a uniform stream. The simulation is truly a DAS approach in which the aerodynamic and acoustic fields are resolved simultaneously. The Reynolds number specified for the range of M investigated is 1.0×10^3. Altogether nine different inlet flows are investigated, and these range from $M = 0.01$ to 0.9. The exact choices of M are listed in Table 1. The same Gaussian sound pulse is specified, and it is defined as

$$\rho = \rho_0 + \sigma \exp\left(- \ell_n 2 \times \frac{(x + 1)^2 + y^2}{0.2^2} \right) \tag{21a}$$

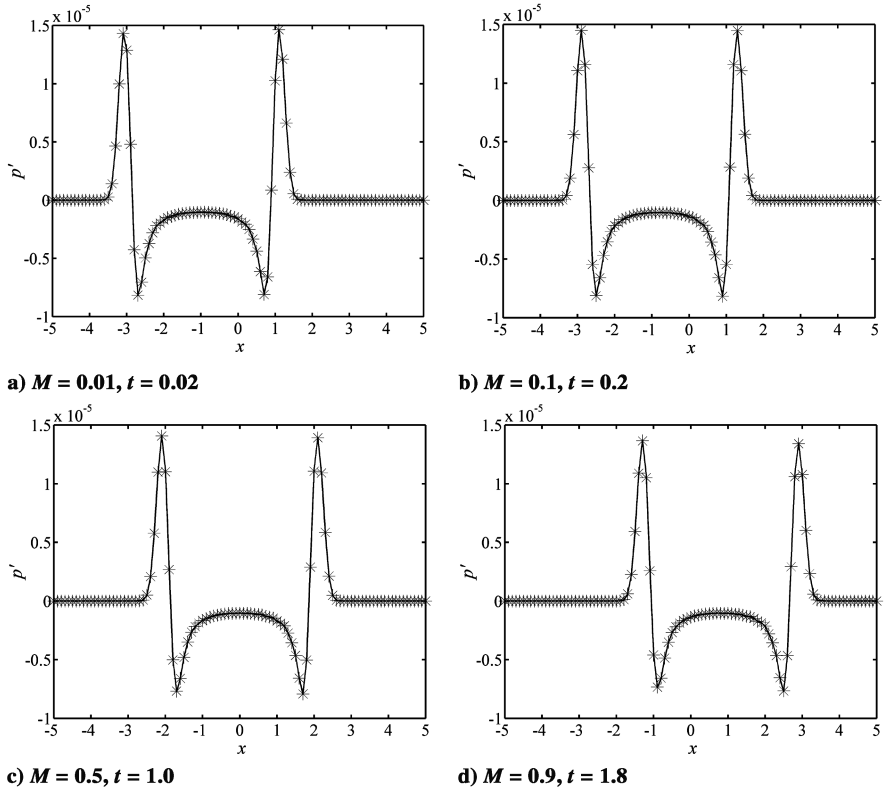

Fig. 2 Instantaneous pressure fluctuations $p' = p - p_0$ along the x axis.

$$u = u_0 \tag{21b}$$

$$v = v_0 \tag{21c}$$

$$p = p_0 + \frac{1}{M^2}\sigma \exp\left(-\ell_n 2 \times \frac{(x+1)^2 + y^2}{0.2^2}\right) \tag{21d}$$

where the inlet conditions are given by $\rho_0 = 1$, $u_0 = 1$, $v_0 = 0$, and $p_0 = 1/\gamma M^2$ and $\sigma = 10^{-4}$ is chosen for the present calculations. The accuracy of the numerical scheme used to solve the DNS and LBM equations has already been demonstrated in Fig. 1.

The objective of the present study is to show that c can be recovered correctly using the modified LBM, and the theoretical relation between c and e is validated. To verify that this is the case, two different ways of estimating c are proposed: One method is to determine c by tracking the speed with which the peaks of the pulse move away from each other, and the second method is to calculate c from Eq. (18). Some sample plots of the pressure pulse for four M cases are shown in Fig. 2. These plots further show that the DNS and the LBM results are essentially identical. From these plots, the distance S between the peaks can be determined, and because the time lapse is known, the speed with which the peaks moved away from each other can be determined. The calculations are carried out for different S and t, and sample plots for $M = 0.01$ and 0.9 are shown in Fig. 3. In this figure is also shown the least-squares fit of all the S and t points chosen for the two M cases presented. These results show very small error in the determination of c by this method.

From the calculated aerodynamic and acoustic fields, p, ρ, and e are known. The p and ρ values can be substituted into Eq. (18) to determine c, and the c thus determined can be plotted against the expression for γ and e. The plots of c versus M for the two different ways of determining c are given in Figs. 4 and 5. The plot of c versus e for a diatomic gas, where $\gamma = 1.4$, is shown in Fig. 6. In these plots,

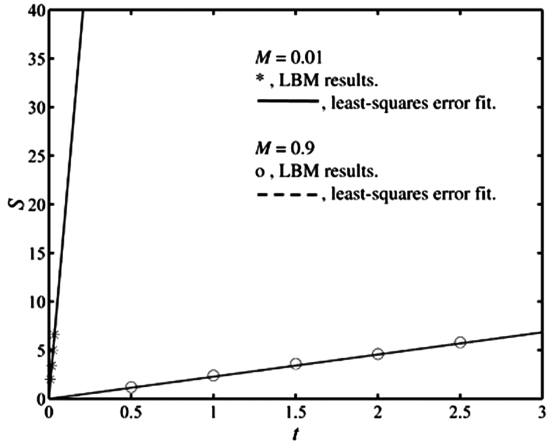

Fig. 3 A plot of the distance S between two maximum peaks versus time t.

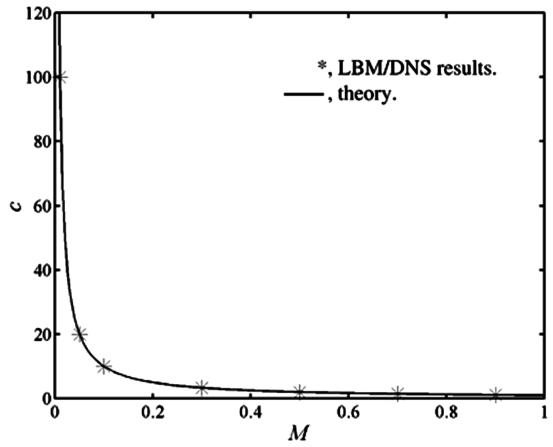

Fig. 4 A plot of the propagation speed of sound $c = \sqrt{\gamma p/\rho}$ versus Mach number M.

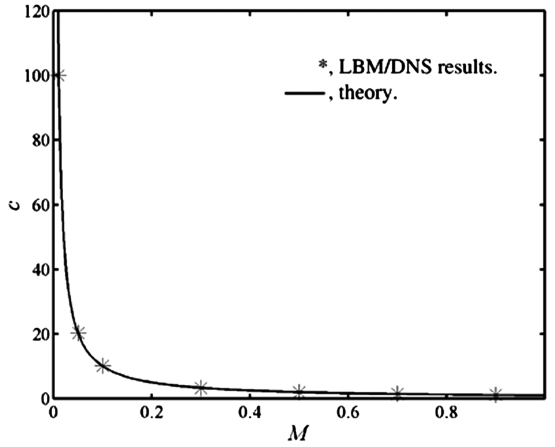

Fig. 5 A plot of the propagation speed of the wave c versus Mach number M.

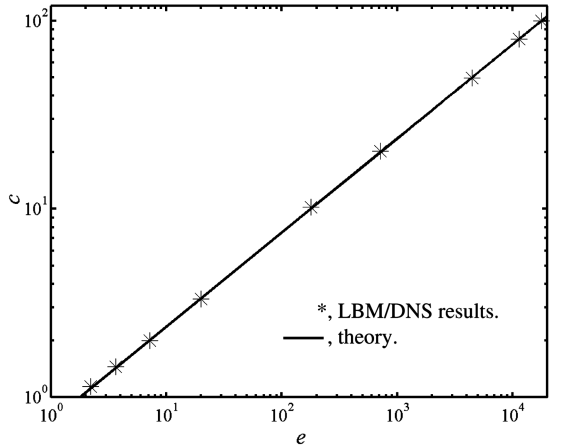

Fig. 6 A plot of the internal energy e versus the propagation speed of sound c.

the DNS and LBM results are denoted by symbols whereas the theoretical analysis is represented by a solid curve. The errors in the determination of c compared with the theoretical values are listed in Table 1. It can be seen that a maximum error of 2.7% occurs in the $M = 0.9$ case; all other cases have errors $\leq 2\%$. This error could be attributed to the lattice and grid sizes chosen. By varying these lattice and grid sizes, a reduced error would result. In the present study, optimal lattice and grid sizes have not been systematically determined. However, the lattice and grid sizes were determined by putting the emphasis on obtaining stable solutions, and this seems to yield very small errors in the whole calculation (Table 1). In fact, the same error is calculated for the DNS and LBM schemes. This implies that the error is more dependent on Δx than on δx. The agreement between theoretical analysis and the DNS and LBM results is excellent (Figs. 4–6). Both the aerodynamic and acoustic fields are resolved correctly within this M range and Reynolds number investigated.

The same LBM has been used to calculate three cases at different M with and without mean flow [31]. These cases are 1) a plane pressure pulse, 2) a circular pressure pulse, and 3) the propagation of acoustic, entropy, and vorticity pulses in a uniform stream. All the problems tested were wave propagation in an infinite medium. No solid boundary is present. Very good agreement between LBM simulations and DNS calculations is obtained.

Previous theoretical analysis [40] with hexagonal lattice shows that linear wave propagation in a lattice gas model is anisotropic and the propagating wave front is distorted with a magnitude depending on wave frequency. The LBM results of cases 2 and 3 in Li et al. [31], as well as all calculations in the present paper, correctly predict a

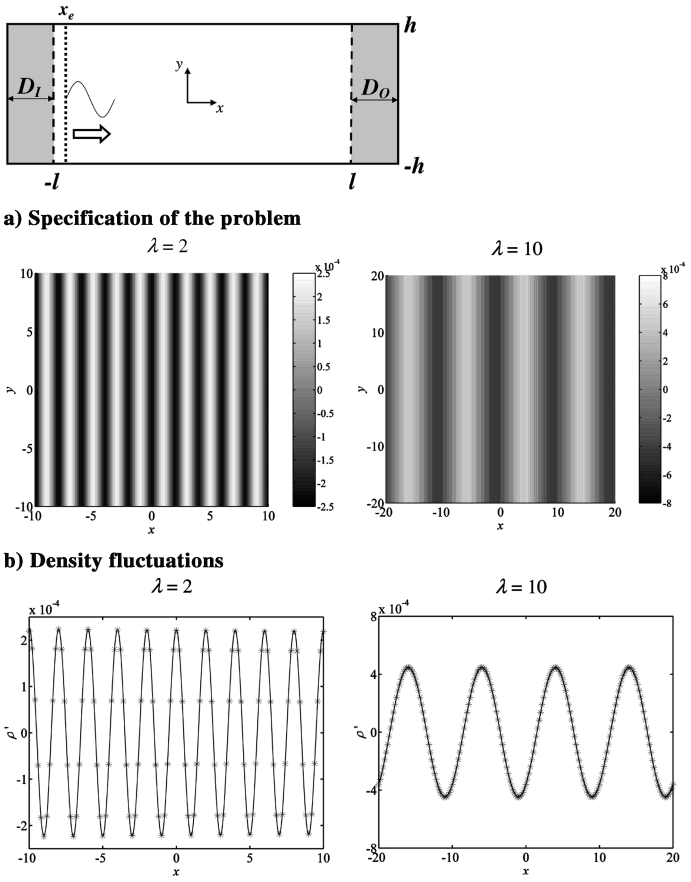

Fig. 7 Propagation of the sound wave in the x direction.

circular expansion of the acoustic pressure pulses. No distortion of the wave front is observed. This shows that sound propagation in the present LBM model is truly isotropic. This property is extremely important in any 2D DAS. Propagation anisotropy, even though a weak one, could lead to incorrect calculations of the interaction between sound and flow, and consequently the error in overall radiating power prediction would be significant.

To verify the frequency independence of the isotropic property of the LBM model, one more case of plane sinusoidal wave propagation in quiescent fluid is calculated. The computational domain size of the problem is $-l \le x \le l$ by $-h \le y \le h$ (Fig. 7a). The same uniform grid (of size 0.02×0.02) as that used in Li et al. [31] is adopted. Two kinds of nonreflecting boundary conditions proposed by Kam et al. [41] are used. On the upper and lower boundaries, an extrapolation method with continuity for the first derivative of f invoked is applied across the boundary. The ABC is adopted on the inlet and outlet boundaries with two buffer regions having size $D_I = 1$ and $D_O = 1$, respectively. The initial conditions of the fluid are $\rho = \rho_\infty$, $u = v = 0$, and $p = p_\infty = 1/\gamma$. On the other hand, $Re = 1.0 \times 10^3$ and $M = 0.1$ are specified. The wave is generated by a weak line sinusoidal pressure excitation with amplitude ε_p and wavelength λ:

$$p = p_\infty[1 + \varepsilon_p \sin(\omega t)] \tag{22}$$

where $\omega = 2\pi c/\lambda$. The excitation location x_e is one grid from $x = -l$. Two calculations are performed, and the calculated density fluctuations are shown in Fig. 7. One is excited with $\lambda = 2$ and $\varepsilon_p = 10^{-5}$, another is with $\lambda = 10$ and $\varepsilon_p = 1.8 \times 10^{-4}$. Evidently the present LBM scheme is truly isotropic and no distortion in sound propagation is observed (Fig. 7b). Furthermore, very good agreement between LBM and DNS simulations are obtained (Fig. 7c). These cases show that the modified LBM scheme is a valid alternative to the DNS scheme in DAS calculations for M varying from 0.01 to 0.9 and for different types of aeroacoustic problems.

V. Conclusions

A BGK model with two relaxation time scales is used to approximate the collision term in the Boltzmann equation. The time scales are chosen to represent the phenomenon of fluid viscosity to account for the momentum transfer between gas particles before and after collisions properly. Thus formulated, the Boltzmann equation can be shown to recover the unsteady compressible Navier–Stokes equations with the dynamic viscosity having the correct dependence on temperature, and γ for a diatomic gas is determined to be exactly 1.4. This modified LBM is used to calculate the aerodynamic and acoustic fields of a Gaussian sound pulse in a uniform stream simultaneously. The inlet Reynolds number is set at 1.0×10^3, and the inlet M vary from 0.01 to 0.9. It is assumed that there is no shock present in the range of M. A DNS scheme is also used to simulate the same problem to provide a benchmark for the LBM approach. The results of both the DNS and LBM approaches are compared with theoretical analysis. Comparisons are made with c versus M and c versus e. Two different ways of determining c from the numerical calculations are carried out: one from the calculated p and γ over the whole field and another from the determination of the speed with which the peaks of the pulse are moving away from each other. Both methods give identical results for c. The DNS results are the same as the LBM results, and both are in excellent agreement with the theoretical results. The maximum error in the determination of c compared with the theoretical value is 2.7%, and it occurs at $M = 0.9$. For all other M cases, the error is either zero or less than 2.7%. In addition, the sound propagation with long ($\lambda = 10$) and short ($\lambda = 2$) wavelengths is calculated. The agreement between LBM and DNS results are excellent. There is no distortion of wave fronts in the solutions. This is further evidence that the present LBM, like the DNS, is truly isotropic. Therefore, the modified LBM is valid for the M range from 0.01 to 0.9 and is a true alternative to DNS for DAS calculations of the aerodynamic and acoustic fields simultaneously.

Acknowledgements

Funding support received from the Research Grants Council of the Government of the Hong Kong Special Administrative Region (through Grants No. PolyU 1/02C, No. PolyU 5174/02E, and No. PolyU 5303/03E) and from the Hong Kong Polytechnic University (through Grant No. A-PF32) is gratefully acknowledged.

References

[1] Tam, C. K. W., "Computational Aeroacoustics: Issues and Methods," *AIAA Journal*, Vol. 33, No. 10, 1995, pp. 1788–1796.
[2] Lele, S. K., "Computational Aeroacoustics: A Review," AIAA Paper 1997-0018, 1997.
[3] Lighthill, J. M., "On Sound Generated Aerodynamically: I General Theory," *Proceedings of the Royal Society of London, Series A: Mathematical and Physical Sciences*, Vol. 211, No. 1107, 1952, pp. 564–587.
[4] Bogey, C., and Bailly, C., "Three-Dimensional Non-Reflective Boundary Conditions for Acoustics Simulations: Far Field Formulation and Validation Test Cases," *Acta Acustica*, Vol. 88, No. 4, 2002, pp. 463–471.
[5] Bailly, C., and Bogey, C., "Contributions of Computational Aeroacoustics to Jet Noise Research and Prediction," *International Journal of Computational Fluid Dynamics*, Vol. 18, No. 6, 2004, pp. 481–491.
[6] Bogey, C., and Bailly, C., "A Family of Low Dispersive and Low Dissipative Explicit Schemes for Flow and Noise Computations," *Journal of Computational Physics*, Vol. 194, No. 1, 2004, pp. 194–214.
[7] Lele, S. K., "Compact Finite Difference Schemes with Spectral-Like Resolution," *Journal of Computational Physics*, Vol. 103, No. 1, 1992, pp. 16–42.
[8] Tam, C. K. W., "Advances in Numerical Boundary Conditions for Computational Aeroacoustics," *Journal of Computational Acoustics*, Vol. 6, No. 4, 1998, pp. 377–402.
[9] Colonius, T., Lele, S. K., and Moin, P., "Boundary Conditions for Direct Computation of Aerodynamic Sound Generation," *AIAA Journal*, Vol. 31, No. 9, 1993, pp. 1574–1582.
[10] Freund, J. B., "Proposed Inflow/Outflow Boundary Condition for Direct Computation of Aerodynamic Sound," *AIAA Journal*, Vol. 35, No. 4, 1997, pp. 740–742.
[11] Hu, F. Q., "A Stable, Perfectly Matched Layer for Linearized Euler Equations in Unsplit Physical Variables," *Journal of Computational Physics*, Vol. 173, No. 2, 2001, pp. 455–480.
[12] Freund, J. B., "Noise Source in a Low Reynolds Number Turbulent Jet at Mach 0.9," *Journal of Fluid Mechanics*, Vol. 438, July 2001, pp. 277–305.
[13] Huteau, F., Lee, T., and Mateescu, D., "Flow Past a 2-D Backward-Facing Step with an Oscillating Wall," *Journal of Fluids and Structures*, Vol. 14, No. 5, 2000, pp. 691–696.
[14] Rowley, C. W., Colonius, T., and Basu, A. J., "On Self-Sustained Oscillations in Two-Dimensional Compressible Flow over Rectangular Cavities," *Journal of Fluid Mechanics*, Vol. 455, March 2002, pp. 315–346.
[15] Gloerfelt, X., Bailly, C., and Juvé, D., "Direct Computation of the Noise Radiated by a Subsonic Cavity Flow and Application of Integral Methods," *Journal of Sound and Vibration*, Vol. 266, No. 1, 2003, pp. 119–146.
[16] Harris, S., *An Introduction to the Theory of the Boltzmann Equation*, Dover, New York, 1999.
[17] Wolf-Gladrow, D. A., *Lattice-Gas Cellular Automata and Lattice Boltzmann Models: An Introduction*, Springer–Verlag, New York, 2000.
[18] Qian, Y. H., dèHumières, D., and Lallemand, P., "Lattice BGK Models for Navier–Stokes Equation," *Europhysics Letters*, Vol. 17, No. 6, 1992, pp. 479–484.
[19] Chen, S., and Doolen, G. D., "Lattice Boltzmann Method for Fluid Flows," *Annual Review of Fluid Mechanics*, Vol. 30, Jan. 1998, pp. 329–364.
[20] Sun, C., "Lattice-Boltzmann Models for High Speed Flow," *Physical Review E*, Vol. 58, No. 6, 1998, pp. 7283–7287.
[21] Palmer, B. J., and Rector, D. R., "Lattice Boltzmann Algorithm for Simulating Thermal Flow in Compressible Fluids," *Journal of Computational Physics*, Vol. 161, No. 1, 2000, pp. 1–20.
[22] Tsutahara, M., Kataoka, T., Takada, N., Kang, H. K., and Kurita, M., "Simulations of Compressible Flows by Using the Lattice Boltzmann and the Finite Difference Lattice Boltzmann Methods," *Computational Fluid Dynamics Journal*, Vol. 11, No. 1, 2002, pp. 486–493.

[23] Kang, H. K., Ro, K. D., Tsutahara, M., and Lee, Y. H., "Numerical Prediction of Acoustic Sounds Occurring by the Flow Around a Circular Cylinder," *KSME International Journal*, Vol. 17, No. 8, 2003, pp. 1219–1225.
[24] Ricot, D., Maillard, V., and Bailly, C., "Numerical Simulation of Unsteady Cavity Flow Using Lattice Boltzmann Method," AIAA Paper 2002-2532, 2002.
[25] Wilde, A., "Calculation of Sound Generation and Radiation from Instationary Flows," *Computers and Fluids*, Vol. 35, No. 8–9, 2006, pp. 986–993.
[26] Danforth, A. L., and Long, L. N., "Nonlinear Acoustic Simulations Using Direct Simulation Monte Carlo," *Journal of the Acoustical Society of America*, Vol. 116, No. 4, 2004, pp. 1948–1955.
[27] He, X., and Luo, L. S., "Theory of the Lattice Boltzmann Method: From the Boltzmann Equation to Lattice Boltzmann Equation," *Physical Review E*, Vol. 56, No. 6, 1997, pp. 6811–6817.
[28] Premnath, K. N., and Abraham, J., "Discrete Lattice BGK Boltzmann Equation Computations of Transient Incompressible Turbulent Jets," *International Journal of Modern Physics C*, Vol. 15, No. 5, 2004, pp. 699–719.
[29] Buick, J. M., Greated, C. A., and Campbell, D. M., "Lattice BGK Simulation of Sound Waves," *Europhysics Letters*, Vol. 43, No. 3, 1998, pp. 235–240.
[30] Buick, J. M., Buckley, C. L., Greated, C. A., and Gilbert, J., "Lattice Boltzmann BGK Simulation of Nonlinear Sound Waves: the Development of a Shock Front," *Journal of Physics A: General Physics*, Vol. 33, No. 21, 2000, pp. 3917–3928.
[31] Li, X. M., Leung, R. C. K., and So, R. M. C., "One-Step Aeroacoustics Simulation Using Lattice Boltzmann Method," *AIAA Journal*, Vol. 44, No. 1, 2006, pp. 78–89.
[32] Leung, R. C. K., Li, X. M., and So, R. M. C., "Comparative Study of Non-Reflecting Boundary Condition for One-Step Duct Aero-Acoustics Simulation," *AIAA Journal*, Vol. 44, No. 3, 2006, pp. 664–667.
[33] Visbal, M. R., and Gaitonde, D. V., "High-Order-Accurate Methods for Complex Unsteady Subsonic Flows," *AIAA Journal*, Vol. 37, No. 10, 1999, pp. 1231–1239.
[34] Hu, F. Q., Hussaini, M. Y., and Manthey, J. L., "Low-Dissipation and Low-Dispersion Runge–Kutta Schemes for Computational Acoustics," *Journal of Computational Physics*, Vol. 124, No. 1, 1996, pp. 177–191.
[35] Bhatnagar, P., Gross, E. P., and Krook, M. K., "A Model for Collision Processes in Gases, 1: Small Amplitude Processes in Charged and Neutral One-Component Systems," *Physical Review*, Vol. 94, No. 3, 1954, pp. 515–525.
[36] Yu, D., Mei, R., Luo, L. S., and Shyy, W., "Viscous Flow Computations with the Method of Lattice Boltzmann Equation," *Progress in Aerospace Sciences*, Vol. 39, No. 5, 2003, pp. 329–367.
[37] Ferziger, J. H., and Kaper, H. G., *Mathematical Theory of Transport Processes in Gases*, North-Holland, Amsterdam, 1975.
[38] Chapman, S., and Cowling, T. G., *The Mathematical Theory of Non-Uniform Gases*, Cambridge Univ. Press, New York, 1970.
[39] So, R. M. C., Liu, Y., Cui, Z. X., Zhang, Z. X., and Wang, X. Q., "Three-Dimensional Wake Effects on the Flow-Induced Forces," *Journal of Fluids and Structures*, Vol. 20, No. 3, 2005, pp. 373–402.
[40] Chen, H., Chen, S., and Doolen, G. D., "Sound Wave Propagation in FHP Lattice Gas Automata," *Physics Letters A*, Vol. 140, No. 4, 1989, pp. 161–165.
[41] Kam, E. W. S., So, R. M. C., and Leung, R. C. K., "LBM Simulation of Aeroacoustics and Non-Reflecting Boundary Conditions," *AIAA Journal* (submitted for publication).

C. Bailly
Associate Editor